SCIENTIFIC REPORTS
nature research

OPEN

Magneto-Optical Characteristics of Streptavidin-Coated Fe_3O_4@Au Core-Shell Nanoparticles for Potential Applications on Biomedical Assays

Chin-Wei Lin[1], Jian-Ming Chen[2], You-Jun Lin[2], Ling-Wei Chao[2], Sin-Yi Wei[2], Chiu-Hsien Wu[2,3], Chien-Chung Jeng[2,3], Li-Min Wang[1] & Kuen-Lin Chen[2,3*]

Recently, gold-coated magnetic nanoparticles have drawn the interest of researchers due to their unique magneto-plasmonic characteristics. Previous research has found that the magneto-optical Faraday effect of gold-coated magnetic nanoparticles can be effectively enhanced because of the surface plasmon resonance of the gold shell. Furthermore, gold-coated magnetic nanoparticles are ideal for biomedical applications because of their high stability and biocompatibility. In this work, we synthesized Fe_3O_4@Au core-shell nanoparticles and coated streptavidin (STA) on the surface. Streptavidin is a protein which can selectively bind to biotin with a strong affinity. STA is widely used in biotechnology research including enzyme-linked immunosorbent assay (ELISA), time-resolved immunofluorescence (TRFIA), biosensors, and targeted pharmaceuticals. The Faraday magneto-optical characteristics of the biofunctionalized Fe_3O_4@Au nanoparticles were measured and studied. We showed that the streptavidin-coated Fe_3O_4@Au nanoparticles still possessed the enhanced magneto-optical Faraday effect. As a result, the possibility of using biofunctionalized Fe_3O_4@Au nanoparticles for magneto-optical biomedical assays should be explored.

Over the past few decades, nanotechnology has advanced rapidly. The special property of unique size of nanoparticles provides many advantages. Magnetic nanoparticles (MNPs) have been developed in many fields, such as biomedicine[1–5], nano fluids[6], magnetic resonance imaging[7–9], and optics[10]. MNPs have recently attracted more attention for biomedical applications because of their magnetic and optical characteristics. MNPs can serve as drug carriers[11], biosensors[12,13], gene delivery systems[14], etc.[15].

Iron oxide MNPs are the most commonly used MNPs due to their superparamagnetic stability and biocompatibility[16]. The properties of Fe_3O_4 MNPs, such as size and shape, can be altered with different synthesis methods[17] and as a result the MNPs can be specialized for different applications. Several synthesis routes have been reported including thermal decomposition[18], co-precipitation[19], and hydrothermal synthesis[20]. Each technique fits the demands of different biomedicine applications. Generally, the particle size of Fe_3O_4 MNPs is affected by pH variation[21], temperature[22], and stirring rate[23] during the synthesis process.

To increase the stability and biocompatibility, the surface of the MNP generally needs to be modified with some noble metal or polymer. Several methods to modify MNPs made of iron oxide have been reported[3,4,24,25]. Gold, a noble metal with good biocompatibility, is commonly used in biomedical applications. Due to their biocompatibility gold coated MNPs have been developed and widely studied[26,27]. Moreover, gold coated MNPs simultaneously possess magnetic and plasmonic characteristics. Jain *et al.* reported that the magneto-optical Faraday effect in gold-coated iron oxide nanocrystals was enhanced due to surface plasmon resonance enhanced magneto-optics (SuPREMO)[28]. However, the nanoparticle surface generally needs to be modified with biomaterials or proteins for applications in biomedicine. It is well known that surface plasmon resonance (SPR) is very

[1]Graduate institute of applied physics, National Taiwan University, Taipei, Taiwan. [2]Institute of Nanoscience, National Chung Hsing University, Taichung, Taiwan. [3]Department of Physics, National Chung Hsing University, Taichung, Taiwan. *email: klchen@phys.nchu.edu.tw

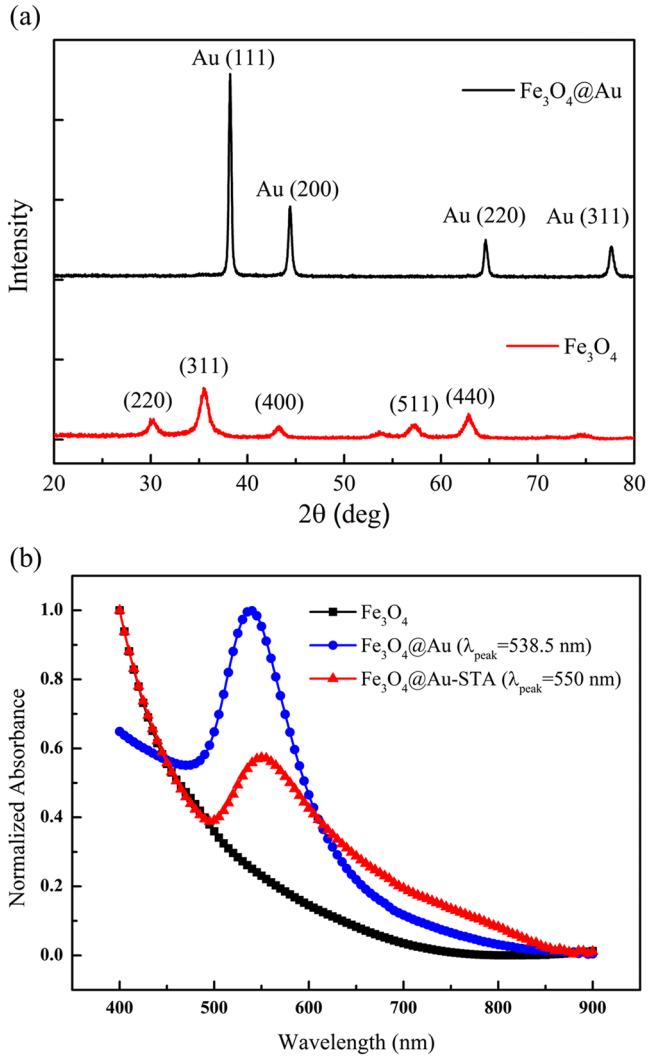

Figure 1. (**a**) Powder XRD patterns and (**b**) UV-Vis spectra of the Fe_3O_4, Fe_3O_4@Au core-shell and Fe_3O_4@Au-STA MNPs.

sensitive to the surface state of the nanoparticle. The SPR of a nanoparticle is highly responsive to small changes in the local refraction index[29]. Hence, the surface modification of biomaterials certainly alters the characteristics of the SPR.

In this work, we synthesized Fe_3O_4@Au core/shell magnetic nanoparticles and coated their surface with streptavidin (STA) to study how the addition of STA impacted the magneto-optical Faraday effect. STA is a widely used biomaterial for developing new biomedical methods because the conjugation of STA and biotin is very strong. It is commonly used to investigate the quantification process with biotin. We experimentally demonstrated that Fe_3O_4@Au core-shell MNPs were still able to enhance the magneto-optical Faraday rotation even after surface modification with STA. This result suggests that SuPREMO is a promising effect to exploit in biomedical assay techniques based on the magneto-optical effect, such as the Faraday immunoassay system[30].

In our previous work[30], we have demonstrated that the Faraday magneto-optical measurement with biofunctionalized magnetic nanoparticles (BMNs) results in a simple, convenient, and sensitive tool for assaying biomarkers. Due to the antibody–antigen interactions, BMNs conjugated with the biotargets to form large magnetic clusters over time. The magnetic characteristics of the BMNs reagent are altered as well. The Faraday rotation angle varies as a function of the size of the MNP. Therefore, we aim to observe the clustering process by measuring the Faraday effect of MNPs. Since SuPRMO MNPs possess the special characteristic of Faraday rotation enhancement, biofunctionalized SuPRMO MNPs are a potential reagent for increasing the sensitivity of the magneto-optical Faraday immunoassay technique.

Results and Discussions

X-ray diffraction (XRD) & UV-Vis spectrum. Figure 1a shows the powder X-ray diffraction (XRD) patterns of Fe_3O_4 and Fe_3O_4@Au core-shell MNPs. The diffraction angle of the (311) peak of the raw MNPs occurs at 35.46°, which means that the composition of the MNPs is magnetite before reducing the Au shell[31]. The XRD data showed that the synthesized particles are Fe_3O_4 with good crystallinity. After coating the MNPS

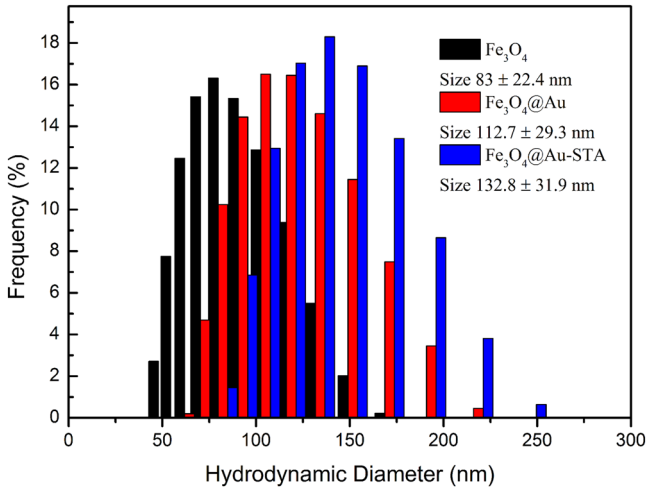

Figure 2. Distribution of the hydrodynamic diameter of the Fe_3O_4, Fe_3O_4@Au core-shell and Fe_3O_4@Au-STA MNPs.

MNPs	Size(nm)	PI	Zeta Potential(mV)
Fe_3O_4	83.0 ± 22.4	0.258	−66.1
Fe_3O_4@Au	112.7 ± 29.3	0.300	−57.8
Fe_3O_4@Au-STA	132.8 ± 31.9	0.338	−46.8

Table 1. Hydrodynamic diameter, polydispersity index (PI) and Zeta potential of the Fe_3O_4, Fe_3O_4@Au, and Fe_3O_4@Au-STA MNPs.

with an Au shell, the XRD signals of the Fe_3O_4 core were shielded by the gold layer because of the heavy atom effect[24]. The absorbance of the synthesized particles was measured using ultraviolet-visible spectroscopy (UV-Vis) (U-2800A, HITACHI). The UV-Vis spectra (Fig. 1b) shows that the absorbance of pure Fe_3O_4 MNPs monotonically decreased with the wavelength of light. However, the Fe_3O_4@Au core-shell MNPs exhibited an absorption peak at a wavelength of approximately 538.5 nm due to the SPR effect of the gold layer. After the bonding of STA, the wavelength of the absorption peak of the Fe_3O_4@Au-STA MNPs increased to around 550 nm. The result clearly shows that the STA modification induces a red shift of the UV-Vis spectrum. This means that the refractive index of the STA does indeed alter the SPR condition of the Fe_3O_4@Au MNPs.

Dynamic light scattering. Figure 2 shows the hydrodynamic sizes of the Fe_3O_4, Fe_3O_4@Au core-shell, and Fe_3O_4@Au-STA MNPs measured by dynamic light scattering (DLS) (SZ-100Z, HORIBA). Table 1 shows the hydrodynamic diameter, polydispersity index (PI), and Zeta potential of the Fe_3O_4, Fe_3O_4@Au, and Fe_3O_4@Au-STA MNPs. The average hydrodynamic diameters of Fe_3O_4, Fe_3O_4@Au, and Fe_3O_4@Au-STA MNPs are 83.0 ± 22.4, 112.7 ± 29.3, and 132.8 ± 31.9 nm, respectively. As expected, the mean size and dispersion of the distribution of the MNPs increases as the amount of covering material increases. The Zeta potential data show that the Fe_3O_4, Fe_3O_4@Au, and Fe_3O_4@Au-STA are both stable in the solution.

High-resolution transmission electron microscopy (HRTEM). Figure 3a presents a high-resolution transmission electron microscopy (HRTEM) (JEM-2010, JEOL Co. Ltd) image of the Fe_3O_4@Au core-shell MNPs. It shows that the shape of the synthesized MNPs was approximately spherical and their average size was about 66 nm. Figure 3b shows a magnified HRTEM image near the surface of a Fe_3O_4@Au core-shell MNP. The crystal structure of the gold shell on the Fe_3O_4 core can be clearly seen. The TEM image simultaneously shows the Au lattice near the particle surface and the Fe_3O_4 lattice at the core. The Fe_3O_4 lattice is relatively blurry because the electron beam has difficulty penetrating to the center of particle. The analysis of the energy-dispersive X-ray spectroscopy (EDS) (JEM-2010, JEOL Co. Ltd) for the Fe_3O_4@Au core-shell MNPs clearly revealed that the synthesized particles contained the elements Fe, O, and Au (Fig. 3c). The results of characteristic analysis proved that the Fe_3O_4@Au core-shell MNPs were successfully synthesized.

Magnetization curve. Figure 4a shows the magnetization curve of the Fe_3O_4@Au MNP reagent measured by a SQUID magnetic property measurement system (MPMS, Quantum Design, Inc) at 300 K. The inset in Fig. 4a shows that there was no hysteresis in the magnetization curve even under a small magnetic field. Fe_3O_4@Au MNPs exhibited the characteristics of superparamagnetic material; noting that the magnetization shown is the magnetization of the MNP reagent, not the magnetization of the MNP powder. A 3-D Nanometer Scale Raman PL Microspectrometer (Tokyo Instruments, INC.) was used to determine whether STA was successfully coated

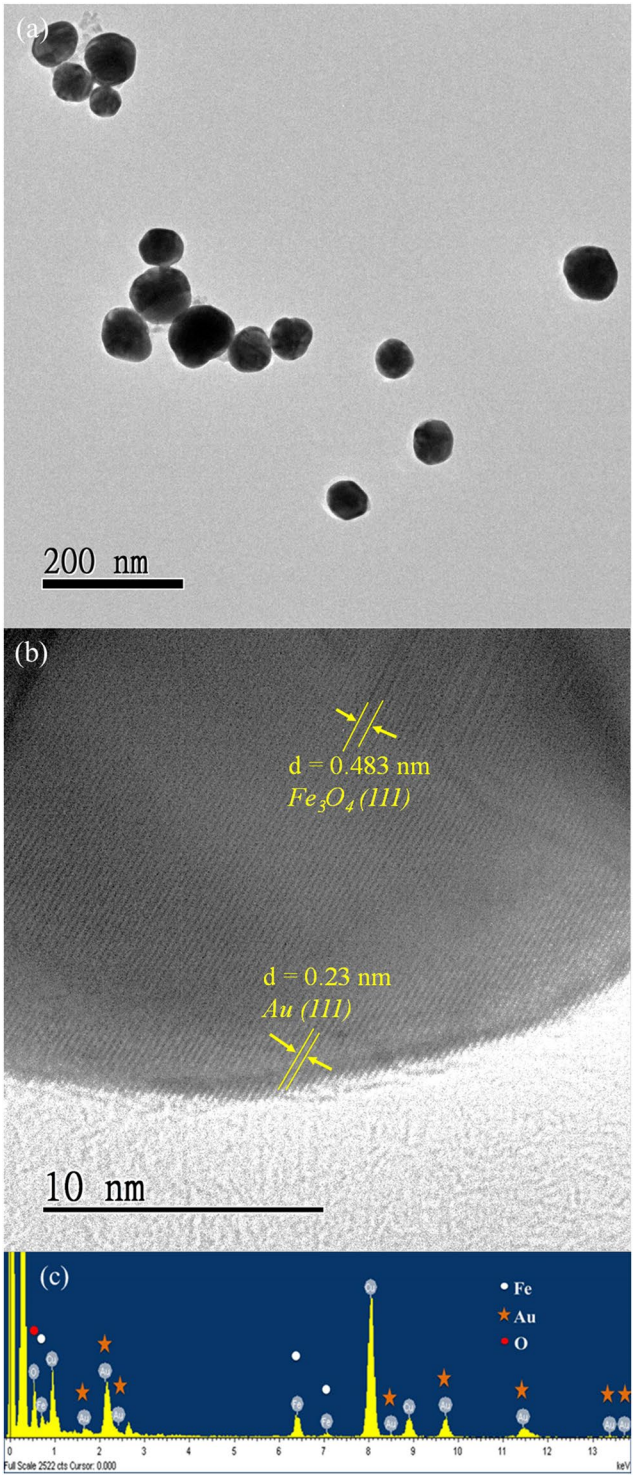

Figure 3. (**a**) TEM images of the Fe_3O_4@Au MNPs. The scale bar is 200 nm. (**b**) Magnified image of the gold shell on the Fe_3O_4 core. The scale bar is 10 nm. (**c**) EDS spectrum of the Fe_3O_4@Au MNPs.

on the surface of Fe_3O_4@Au MNPs. Figure 4b shows the Raman spectra of the Fe_3O_4@Au MNPs before and after coating STA. After STA was coated, peaks emerged in the region of 1200–1600 cm^{-1} with respect to the Raman signals of Fe_3O_4@Au MNPs. The marked peaks in Fig. 4b showed the presence of STA. Peaks at 1254 and 1279 cm^{-1} represent the amide III region and the peak at 1447 cm^{-1} represents the δ-CH_2 and δ-CH_3 bands. The Trp10, Trp7, Trp5, and Trp2 signals are at 1243, 1341, 1461, and 1580 cm^{-1}, respectively[32]. All these peaks are the characteristic Raman signals of STA[32] indicating that STA was successfully coated on the surface of the Fe_3O_4@Au MNPs.

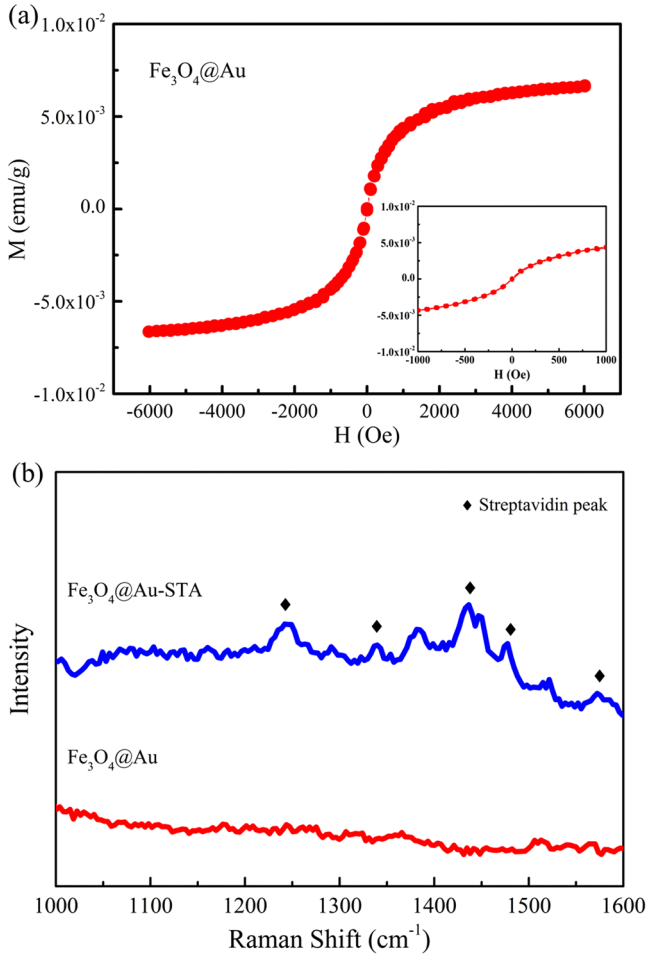

Figure 4. (**a**) Magnetic hysteresis curve of the Fe_3O_4@Au MNPs. The inset shows the magnetization of the Fe_3O_4@Au MNPs under a small magnetic field. (**b**) Raman spectra of the Fe_3O_4@Au MNPs before and after coating STA. The markers indicate the characteristic Raman peaks of STA.

Faraday rotation measurement. To confirm the Faraday rotation enhancement of the Fe_3O_4@Au-STA MNPs, we checked the magneto-optical characteristic of the pure STA reagent. Figure 5a is the Faraday rotation spectrum of pure STA reagent (100 μg/mL) as a function of the applied magnetic field. Clearly the magneto-optical Faraday effect of the pure STA reagent was extremely weak when the applied magnetic field was less than 100 gauss. Recalling that Fig. 1b revealed that the STA modification does indeed alter the SPR condition of the Fe_3O_4@Au NPs; Fig. 5b shows the Faraday rotation spectra of the Fe_3O_4@Au-STA and Fe_3O_4 MNPs reagents as a function of the applied magnetic field. To exclude the influence of magnetization on the Faraday rotations, the saturation magnetizations of the measured samples were controlled ($M_s = 6.6 \times 10^{-3}$ emu/g for both). Figure 5b shows that the Faraday rotation of the Fe_3O_4@Au-STA was larger than that of Fe_3O_4 for an applied magnetic field larger than 30 gauss. The gold layer of core shield MNPs can be seen as an optical cavity with multiple resonance modes. When the light at a corresponding frequency illuminates the cavity, the energy of that light is stored inside the cavity. The result is that the MNP inside cavity senses a stronger electromagnetic field than the MNP without a cavity. The enhanced interaction between the MNPs and light results in the larger Faraday rotation. This result proves that the Fe_3O_4@Au-STA MNPs still possessed the SuPREMO effect which enhances the Faraday rotation even after the STA coating was applied. The biomaterial modified magneto-plasmonic nanoparticle is promising for applications based on the magneto-optical Faraday effect. In our previous work[30], we successfully developed a Faraday immunoassay technique based on the magneto-optical Faraday effect and biofunctionalized MNPs. Now, these experimental results suggest that biofunctionalized magneto-plasmonic nanoparticle can be exploited to improve sensitivity using the Faraday immunoassay technique.

In summary, we synthesized the Fe_3O_4@Au core-shell MNPs and coated particle surfaces with STA. We observed that the Fe_3O_4@Au-STA MNPs still possess the Faraday rotation enhancement after conjugating the biomaterial on the surface of the gold layer. The experimental results imply that the biofunctionalized Fe_3O_4@Au core-shell MNPs still had the effect of SuPREMO and are promising for magneto-optical biomedical applications.

Methods Synthesis of the bio-functionalized core-shell Fe_3O_4@Au nanoparticles. In this study, iron oxide nanoparticles were prepared by co-precipitation of Fe(II) and Fe(III) first. An iron salt aqueous solution was combined with Ferric chloride ($FeCl_3.6H_2O$) and ferrous chloride ($FeCl_2.4H_2O$) at a ratio of 2:1. The iron

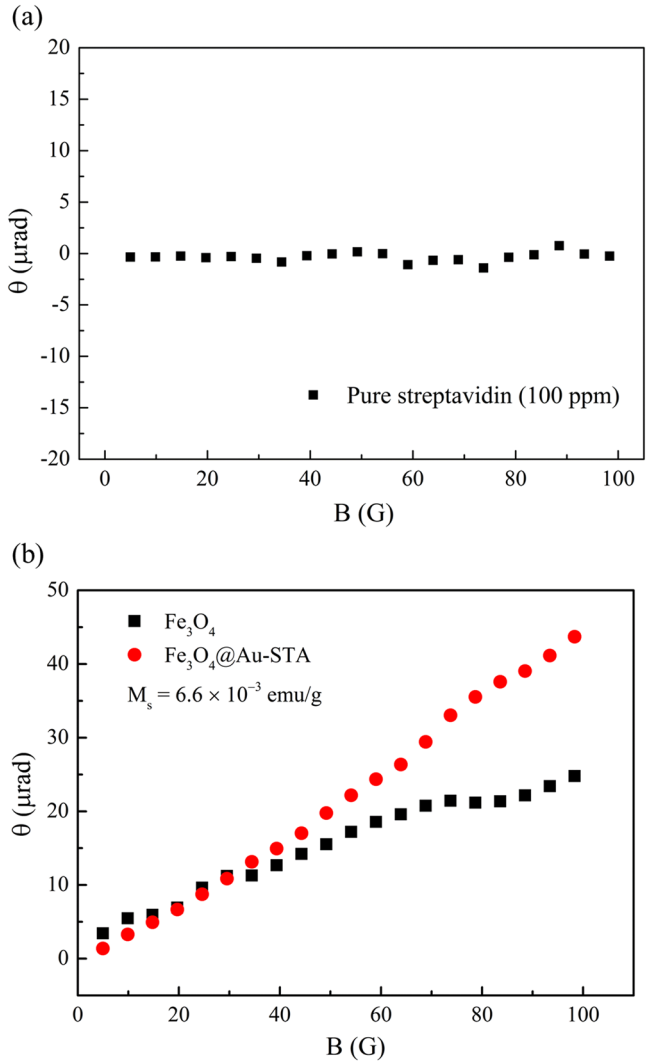

Figure 5. (**a**) Faraday rotation spectrum of the pure STA reagent with the concentration of 100 μg/mL. (**b**) Faraday rotation spectra of Fe_3O_4@Au-STA and Fe_3O_4 MNPs. The saturation magnetizations of the Fe_3O_4@Au-STA and Fe_3O_4 MNPs reagents both were 6.6×10^{-3} emu/g.

salt aqueous solution was heated to 80 °C. Then, 28% NH_4OH (W/V) was added to the iron salt aqueous solution and stirred for 30 min to form Fe_3O_4 nanoparticles. After that, Fe_3O_4 nanoparticles were obtained by magnetic separation. DI water was used to wash the precipitate.

Subsequently, the synthesized Fe_3O_4 MNPs were dispersed in 0.1 M (50 mL) Tetramethylammonium hydroxide (TMAOH) solution. Next, 0.1 mL Fe_3O_4/TMAOH solution and 100 mL DI water were stirred with sodium citrate (0.2 M, 3 mL) to replace surface hydroxide ions with citrate ions. Afterward, 1% (W/V) (0.5 mL) HAuCl4 solution and 0.2 M (0.2 mL) hydroxylamine hydrochloride ($NH_2OH{\cdot}HCl$) were iteratively added to the colloid to reduce the gold shells on the surface of Fe_3O_4 to form Fe_3O_4@Au core-shell MNPs[33]. The mixed colloid was continuously stirred during each iteration. In total 10 iterations were executed and every iteration took 20 minutes. Fe_3O_4@Au MNPs were obtained by centrifuging (6000 rpm, 30 min) and were then washed with DI water. The precipitate Fe_3O_4@Au MNPs were dispersed in ethanol (2 mL).

Surface modification was needed to bind STA onto the gold surface[34]. 11-mercaptoundecanoic acid (11-MUA) can be self-assembled on the gold surface of Fe_3O_4@Au MNPs and provides a carboxyl group for bioconjugation. Fe_3O_4@Au nanoparticles were added with 11-MUA (20 mM, 200 μL) and then continuously sonicated for 20 hours. We then centrifuged (12000 rpm, 10 min) the colloid and washed the precipitate with the ethanol. Afterwards, the precipitate was dissolved into PBS (0.001 M, 1 mL, pH 7.4). To activate the carboxyl groups on the gold surface prior to covalent coupling, N-(3-dimethylaminopropyl)-N'-ethylcarbodiimide hydrochloride (EDC) (20 mM, 200 μL) and n-hydroxysuccinimide (NHS) (40 mM, 200 μL) were added and continuously sonicated for 2 hours. Then the STA (1 mg/1 mL, 50 μL) was added and the mixed solution was sonicated for 1 hour to form Fe_3O_4@Au-STA MNPs. EDC and NHS enable the bioconjugation of carboxyl groups on the gold surface with the amino groups of STA molecules to form the streptavidin-coated Fe_3O_4@Au core-shell MNPs (Fe_3O_4@Au-STA).

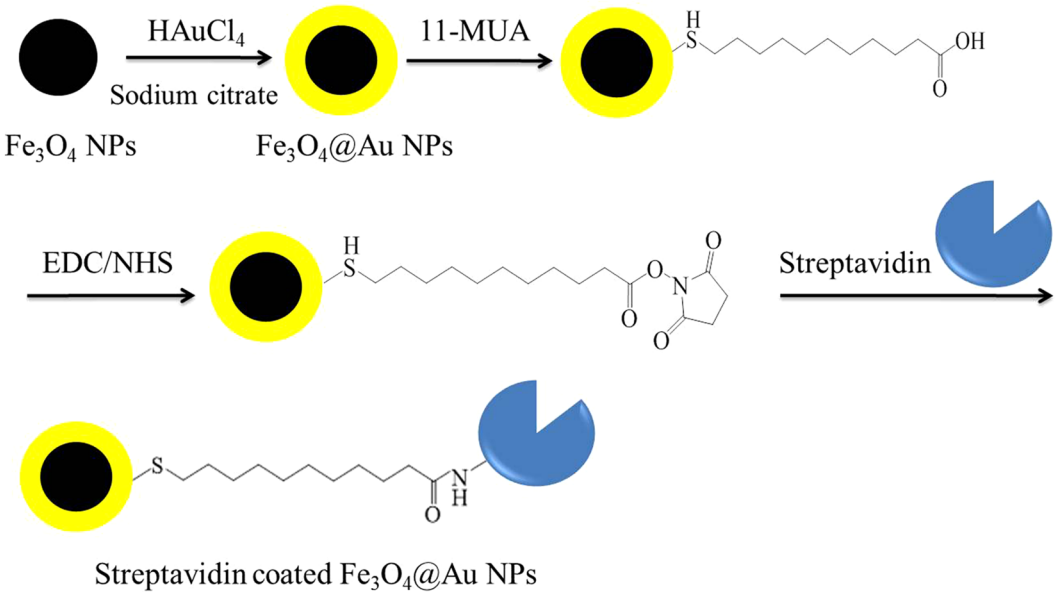

Figure 6. Flow chart of the synthesis process of streptavidin-coated Fe_3O_4@Au core-shell MNPs.

Finally, a liquid phase reagent containing Fe_3O_4@Au-STA MNPs was produced. Figure 6 shows the synthesis processes of Fe_3O_4@Au-STA MNPs.

The Faraday rotation measurement setup. The Faraday rotation measurement was performed using AC magnetic fields and lock-in technique[35,36]. The light source was a diode-pumped solid-state laser with a wavelength of 532 nm. The frequency of the AC magnetic field was set at 813 Hz of which the environment noise was relatively lower. More details of the Faraday rotation measurement can be found in[30]. The measurement samples were prepared in liquid phase and encapsulated in sample holders made of glass. X-ray diffraction (XRD) was performed using BRUKER D8 SSS diffractometer with CuKα radiation.

Received: 1 August 2019; Accepted: 18 October 2019;
Published online: 11 November 2019

References

1. Pankhurst, Q. A., Connolly, J., Jones, S. K. & Dobson, J. Applications of magnetic nanoparticles in biomedicine. *J. Phys. D Appl. Phys.* **36**, 167–181 (2003).
2. Berry, C. C. & Curtis, A. S. G. Functionalisation of magnetic nanoparticles for applications in biomedicine. *J. Phys. D Appl. Phys.* **36**, 198–206 (2003).
3. Xu, C. J. & Sun, S. H. Monodisperse magnetic nanoparticles for biomedical applications. *Polym. Int.* **56**, 821–826 (2007).
4. Xu, C. *et al.* Nitrilotriacetic Acid-Modified Magnetic Nanoparticles as a General Agent to Bind Histidine-Tagged Proteins. *J. Am. Chem. Soc.* **126**, 3392–3393 (2004).
5. Gao, J. *et al.* Intracellular Spatial Control of Fluorescent Magnetic Nanoparticles. *J. Am. Chem. Soc.* **130**, 3710–3711 (2008).
6. Abareshi, M., Goharshadi, E. K., Zebarjad, S. M., Fadafan, H. K. & Youssefi, A. Fabrication, characterization and measurement of thermal conductivity of Fe_3O_4 nanofluids. *J. Magn. Magn. Mater.* **332**, 3895–3901 (2010).
7. Sun, C., Lee, J. S. H. & Zhang, M. Q. Magnetic nanoparticles in MR imaging and drug delivery. *Adv. Drug Deliv. Rev.* **60**, 1252–1265 (2008).
8. Wang, Y. X. J., Hussain, S. M. & Krestin, G. P. Superparamagnetic iron oxide contrast agents: physicochemical characteristics and applications in MR imaging. *Eur. Radiol.* **11**, 2319–2331 (2001).
9. Chertok, B. *et al.* Iron oxide nanoparticles as a drug delivery vehicle for MRI monitored magnetic targeting of brain tumors. *Biomaterials* **29**, 487–496 (2008).
10. Radon, A., Drygala, A., Hawelek, L. & Lukowiec, D. Structure and optical properties of Fe_3O_4 nanoparticles synthesized by co-precipitation method with different organic modifiers. *Mater. Charact.* **131**, 148–156 (2017).
11. Estelrich, J., Escribano, E., Queralt, J. & Busquets, M. A. Iron oxide nanoparticles for magnetically-guided and magnetically-responsive drug delivery. *Int J Mol Sci.* **16**, 8070–8101 (2015).
12. Shi, X. *et al.* Enzymatic biosensors based on the use of metal oxide nanoparticles. *Microchim. Acta.* **181**, 1–22 (2014).
13. Baghayeri, M., Zare, E. N. & Lakouraj, M. M. A simple hydrogen peroxide biosensor based on a novel electro-magnetic poly(p-phenylenediamine)@Fe_3O_4 nanocomposite. *Biosens. Bioelectron.* **55**, 259–265 (2014).
14. Jiang, S., Eltoukhy, A. A., Love, K. T., Langer, R. & Anderson, D. G. Lipoid-coated iron oxide nanoparticles for efficient DNA and siRNA delivery. *Nano Lett.* **13**, 1059–1064 (2012).
15. Nidhin, M., Indumathy, R., Sreeram, K. J. & Nair, B. U. Synthesis of iron oxide nanoparticles of narrow size distribution on polysaccharide templates. *Bull. Mater. Sci.* **31**, 93–96 (2008).
16. Zhu, N. *et al.* Surface modification of magnetic iron oxide nanoparticles. *Nanomaterials* **8**, 810 (2018).
17. Mahdavi, M. *et al.* Synthesis, surface modification and characterisation of biocompatible magnetic iron oxide nanoparticles for biomedical applications. *Molecules.* **18**, 7533–7548 (2013).
18. Sharma, G. & Jeevanandam, P. Synthesis of self-assembled prismatic iron oxide nanoparticles by a novel thermal decomposition route. *RSC Adv.* **3**, 189–200 (2013).

19. Petcharoen, K. & Sirivat, A. Synthesis and characterization of magnetite nanoparticles via the chemical co-precipitation method. *Mater. Sci. Eng. B-Adv.* **177**, 421–427 (2012).
20. Li, H. *et al*. HEPES-involved hydrothermal synthesis of Fe_3O_4 nanoparticles and their biological application. *RSC Adv.* **5**, 5059–5067 (2015).
21. Sun, J. *et al*. Synthesis and characterization of biocompatible Fe_3O_4 nanoparticles. *J Biomed Mater Res A*. **80**, 333–341 (2007).
22. Mahdavi, M., Ahmad, M., Haron, M. J., Rahman, M. Z. & Fatehi, A. Optimized conditions for graft copolymerization of poly(acrylamide) onto rubber wood fiber. *BioResources.* **6**, 5110–5120 (2011).
23. Hua, C. C. *et al*. Size controlled synthesis and characterization of Fe_3O_4 nanoparticles by chemical coprecipitation method. *Sains. Malaysiana* **37**, 389–394 (2008).
24. Xu, C. *et al*. Dopamine as A Robust Anchor to Immobilize Functional Molecules on the Iron Oxide Shell of Magnetic Nanoparticles. *J. Am. Chem. Soc.* **126**, 9938–9939 (2004).
25. Gu, H., Yang, Z., Gao, J., Chang, C. K. & Xu, B. Heterodimers of Nanoparticles: Formation at a Liquid-Liquid Interface and Particle-Specific Surface Modification by Functional Molecules. *J. Am. Chem. Soc.* **127**, 34–35 (2005).
26. Xu, Z. C., Hou, Y. L. & Sun, S. H. Magnetic core/shell Fe_3O_4/Au and Fe_3O_4/Au/Ag nanoparticles with tunable plasmonic properties. *J. Am. Chem. Soc.* **129**, 8698–8699 (2007).
27. Li, J. *et al*. Hyaluronic acid-modified Fe_3O_4@Au core/shell nanostars for multimodal imaging and photothermal therapy of tumors. *Biomaterials* **38**, 10–21 (2015).
28. Jain, P. K., Xiao, Y., Walsworth, R. & Cohen, A. E. Surface Plasmon Resonance Enhanced Magneto-Optics (SuPREMO): Faraday Rotation Enhancement in Gold-Coated Iron Oxide Nanocrystals. *Nano Lett.* **9**, 1644–1650 (2009).
29. Mock, J. J., Smith, D. R. & Schultz, S. Local Refractive Index Dependence of Plasmon Resonance Spectra from Individual Nanoparticles. *Nano Lett* **3**, 485–491 (2003).
30. Chen, K. L. *et al*. A sensitive platform for *in vitro* immunoassay based on biofunctionalized magnetic nanoparticles and magneto-optical Faraday effect. *Sens. actuators. B Chem.* **258**, 947–951 (2018).
31. Zhang, X., Niu, Y., Meng, X., Li, Y. & Zhao, J. Structural evolution and characteristics of the phase transformations between α-Fe_2O_3, Fe_3O_4 and γ-Fe_2O_3 nanoparticles under reducing and oxidizing atmospheres. *Cryst. Eng. Comm.* **15**, 8166–8172 (2013).
32. Galarreta, B. C., Norton, P. R. & Labarthet, F. L. SERS Detection of Streptavidin/Biotin Monolayer Assemblies. *Langmuir* **27**, 1494–1498 (2011).
33. Lyon, J. L., Fleming, D. A., Stone, M. B., Schiffer, P. & Williams, M. E. Synthesis of Fe Oxide Core/Au Shell Nanoparticles by Iterative Hydroxylamine Seeding. *Nano Lett.* **4**, 719–723 (2004).
34. Liu, H. L., Sonn, C. H., Wu, J. H., Lee, K. M. & Kim, Y. K. Synthesis of streptavidin-FITC-conjugated core–shell Fe_3O_4-Au nanocrystals and their application for the purification of CD4+ lymphocytes. *Biomaterials* **29**, 4003–4011 (2008).
35. Jain, A., Kumar, J., Zhou, F., Li, L. & Tripathy, S. A simple experiment for determining Verdet constants using alternating current magnetic fields. *Am. J. Phys.* **67**, 714–717 (1999).
36. Valev, V. K., Wouters, J. & Verbiest, T. Precise measurements of Faraday rotation using ac magnetic fields. *Am. J. Phys.* **76**, 626–629 (2008).

Acknowledgements

The authors would like to acknowledge financial support funded by Ministry of Science and Technology of Taiwan under grants: MOST103-2112-M-005-005-MY3, MOST 106-2112-M-005-002, MOST 107-2112-M-005-012 and MOST 107-2314-B-005-002.

Author contributions

Conceptualization was deduced by K.-L.C.; most of the synthesis and measurements were done by S.-Y.W, C.-W.L., J.-M.C., Y.-J.L., and L.-W.C.; Formal Analysis, J.-M.C., Y.-J.L., and L.-W.C.; Investigation, C.-W.L.; Resources, C.-H.W., C.-C.J., and L.-M.W.; Writing-Original Draft Preparation, C.-W.L., and Y.-J.L.; Writing-Review & Editing, K.-L.C.; Supervision, K.-L.C.; Project Administration, K.-L.C.

Competing interests

The authors declare no competing interests.

Additional information

Correspondence and requests for materials should be addressed to K.-L.C.

Reprints and permissions information is available at www.nature.com/reprints.

Publisher's note Springer Nature remains neutral with regard to jurisdictional claims in published maps and institutional affiliations.